Resonances in Tapered Double-Port TEM Waveguides

Jens Peter Kaerst
HAWK, Fachhochschule Hildesheim/Holzminden/Göttingen
Von-Ossietzky-Str. 99, 37085 Göttingen, kaerst@hawk-hhg.de

Abstract: In this paper resonances in tapered double-port TEM waveguides are used as benchmark for simulations. FEM simulations with COMSOL Multiphysics and simulations using generalised telegraphist's equations with MATLAB are compared to an analytical method capable of calculating the resonances of higher order modes. It is valid for tapered double-port TEM waveguides with constant characteristic impedance. Because these resonances determine the usable bandwidth of the waveguide their precise knowledge is essential. The accuracy of the proposed method has been proven using a TEM waveguides with circular cross section.

Keywords: TEM Waveguide, coupled mode analysis, resonance

1 Introduction

Double port waveguides (e.g. Crawford cell [1]) consist of two tapered sections and a homogeneous middle section. Both ports may be used for measurements, excitation, or resistively loaded. Characteristic cell impedance is usually designed to be $Z_C = 50\,\Omega$ to facilitate connection to standard measurement equipment. Below the geometry dependant cutoff frequencies of higher order modes only the TEM (transverse electromagnetic) mode is able to propagate. Therefore the homogeneous middle section can be used for EMC emission and immunity measurements or to couple electromagnetic energy in or out using an antenna. This concept has been adopted for calibration purposes [2], [3], [4]. In [4] a small circular coaxial calibration cell (μC^3-cell) was introduced in order to overcome the disadvantages of cells with rectangular cross sections (e.g. μTEM-cell). The coaxial circular symmetric geometry avoids an abrupt transition from the circular cross section of the feeding coaxial cable to a rectangular cross section of the cell. This design is optimal with regard not only to low reflection and power loss to unwanted modes, but also in that it simplifies manufacturing and calculations. μTEM and μC^3 cell are depicted in figure 1.

Figure 1: μTEM (left) and μC^3 cell (right)

In an ideal circular coaxial waveguide the coupling between TEM and TE modes is avoided due to symmetry. Therefore the usable bandwidth which is characterised by the desired transverse electromagnetic field is expanded by the factor of three using a circular coaxial waveguide with the same distance between inner and outer conductor for the homogeneous middle section [4]. Referring to the μTEM-cell, the μC^3cell has been constructed such, that this prediction can be proven.

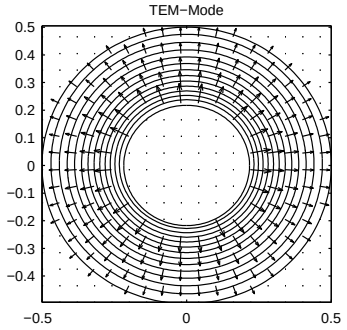

Figure 2: Eigenvector, TEM mode

The transversal $\vec{E}$ field eigenvectors of the TEM mode and the TM$_{01}$ mode are depicted in figure 2 and 3 respectively.

As discussed in [4] and [5] a non ideal geometry or any EUT placed inside the waveguide couples TEM with TE modes, which in turn leads to resonating TE modes. Because of the high quality factor of the resonator a weak coupling (low energy) will already lead to high field amplitudes of resonating higher order modes. The numerical calculation of the coupling coefficients is included in [4] and [6]. In all TEM waveguides with circular cross section (e.g. μC^3) the resonances, sorted by frequency, are TE_{11},TE_{21},...,TM_{01},TM_{11},....

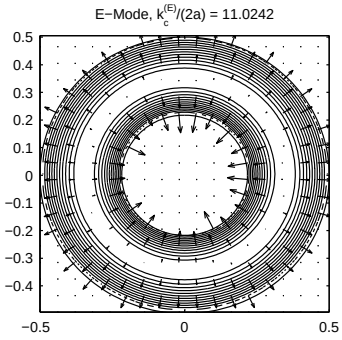

Figure 3: Eigenvector, TM_{01} mode

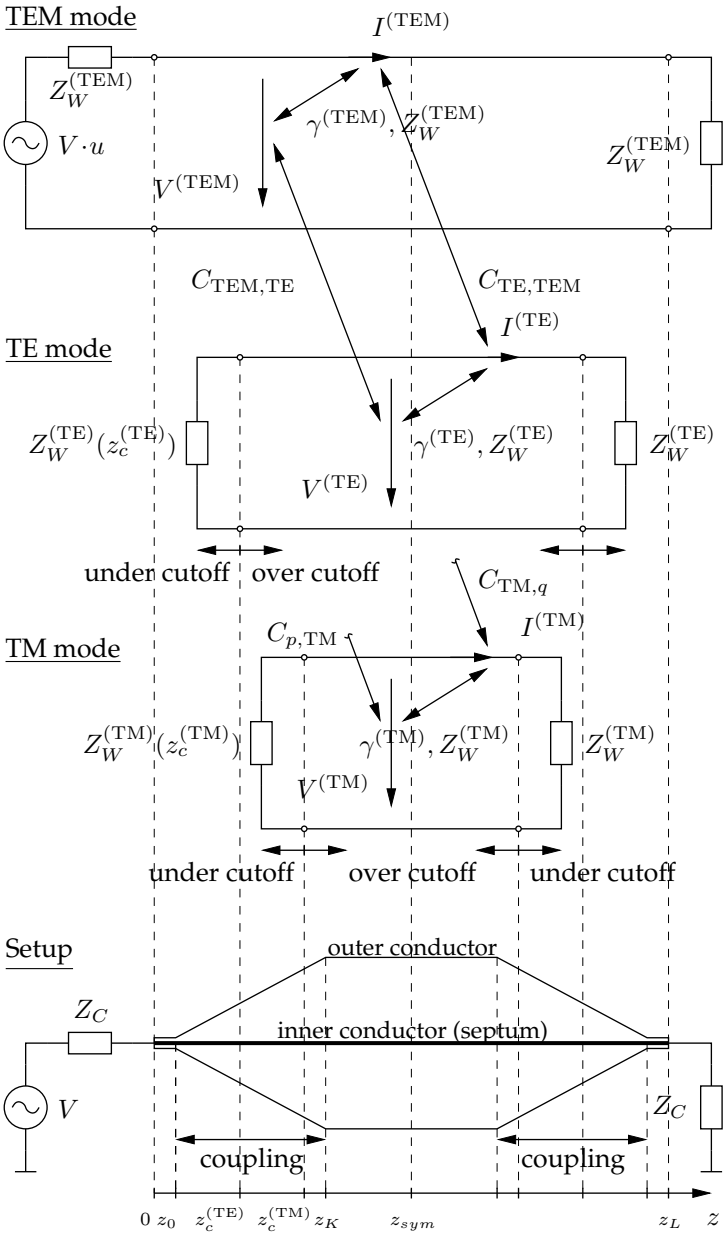

Figure 4: Transmission line model of a tapered double-port TEM

2 Analytical Calculation

The analytical calculation of resonances in tapered double-port TEM waveguides was first published in [5]. It is based on the work included in [7], [8], [9] and [10]. Based on generalised telegraphist's equations the field inside a TEM waveguide is calculated in [4].

The generalised telegraphist's equations for mode p for inhomogeneous waveguides yield

$$\frac{\mathrm{d}V^{(p)}}{\mathrm{d}z} = -\gamma^{(p)}(z)Z_W^{(p)}(z)I^{(p)}(z) + \sum_{q=1}^{\infty} C_{pq}(z)V^{(q)}(z) \quad (1)$$

$$\frac{\mathrm{d}I^{(p)}}{\mathrm{d}z} = -\frac{\gamma^{(p)}(z)}{Z_W^{(p)}(z)}V^{(p)}(z) - \sum_{q=1}^{\infty} C_{qp}(z)I^{(q)}(z) \quad (2)$$

with the propagation constant $\gamma^{(p)}$ and wave impedance $Z_W^{(p)}$ according to table 1 and wave number k. The cutoff wavenumber $k_c^{(p)}$ is a function of the local cross sectional geometry. $V^{(p)}$ and $I^{(p)}$ are historically termed voltage and current coefficients, scaling the associated transversal eigenvectors. The coupling coefficients C_{pq} and C_{qp} quantify energy transfer between modes p and q.

p	TEM	TE	TM
$\gamma^{(p)}$	$\jmath \cdot k$	$\sqrt{k_c^{(p)^2} - k^2}$	
$Z_W^{(p)}$	$\sqrt{\frac{\mu}{\varepsilon}}$	$\frac{\jmath\omega\mu}{\gamma^{(\mathrm{TE})}}$	$\frac{\gamma^{(\mathrm{TM})}}{\jmath\omega\varepsilon}$

Table 1: Propagation constant and wave impedance

Starting with the generalised telegraphist's equations for inhomogeneous waveguides (1) and (2), the resonant frequencies of all higher order modes can be calculated for any coaxial waveguide. The underlying consideration is that resonances are determined by the geometry of the cell and characteristics of the particular mode. Mode coupling means transfer of energy between modes and consequently changes in the field amplitudes, but it does not shift the very resonant frequency.

Essential higher order modes excited by changes of the cross sectional geometry become first able to propagate in the homogeneous middle section of a coaxial cell, whereas in the two tapered sections these modes reach their cutoff cross sections $z_c^{(\mathrm{TE,TM})}(f)$ and are not able to propagate any further, as shown in the transmission line model, figure 4. These cutoff cross sections determine the effective resonance length of the cell wich becomes longer with increasing frequency. At these cutoff cross sections, the power of the mode is reflected. Reflections at cutoff can cause strong field resonances due to the high quality factor of the cell operating as cavity resonator. Thus resonances are always unwanted for EMC measurements as they perturb the desired field distribution normally based on the TEM mode solely.

In figure 4, the coupling between TEM mode and, as an example, two higher order modes is depicted using a Crawford cell. The coupling takes place in regions with varying cross sectional waveguide geometry. With the knowledge of the coupling coefficients, the field amplitudes inside the waveguide can be calculated, as done in [4].

For $k > k_c^{(p)}$ the mode is above cutoff and propagates, whereas for $k < k_c^{(p)}$ the mode is below cutoff and decays exponentially. Because of $k_c^{(\mathrm{TEM})} = 0$, the TEM mode propagates at all frequencies.

As the cross sectional geometry changes along the direction of propagation z, the cutoff frequencies of higher order modes change accordingly. This behaviour can be termed local cutoff frequency. The determination of the local cutoff frequency is simplified if the cross sectional dimensions of the waveguide remain the same in every cross section. This property is termed inherent shape and a calculation is required for one cross section only. For TEM cells, this condition of inherent shape is approximately fulfilled.

The geometry dependent cutoff wave numbers can be determined from normalized wave numbers $k_{c,norm}^{(p)}$ using

$$k_c^{(\mathrm{TE,TM})}(z) = \frac{k_{c,norm}^{(p)}}{2a(z)} \quad . \quad (3)$$

$k_{c,norm}^{(p)}$ is calculated at a cross section with normalised width (rectangular cross section) or outer radius (circular cross section) of the cell chosen to be $2a = 1$ m. The normalised wave numbers are included in [5].

In order to determine solely the resonant frequencies but not the field amplitudes mode coupling in the generalised telegraphist's equations for inhomogeneous waveguides can be disregarded.

Neglecting mode coupling the voltage coefficients for TE modes

$$\frac{\mathrm{d}^2 V_k^{(\mathrm{TE})}}{\mathrm{d}z^2} = \left({k_c^{(\mathrm{TE})}}^2(z) - k^2 \right) V_k^{(\mathrm{TE})}(z) \quad (4)$$

and the current coefficients for TM modes

$$\frac{\mathrm{d}^2 I_k^{(\mathrm{TM})}}{\mathrm{d}z^2} = \left({k_c^{(\mathrm{TM})}}^2(z) - k^2 \right) I_k^{(\mathrm{TM})}(z) \quad (5)$$

can be derived from (1) and (2) using wavenumber $k = \omega\sqrt{\mu\varepsilon}$.

In case of wave propagation exclusively in the TEM mode the physical voltage $V = \frac{V^{(\mathrm{TEM})}}{u}$ and current $I = I^{(\mathrm{TEM})} \cdot u$ can be expressed using the transformation ratio u and the voltage and current coefficients of the TEM mode. The characteristic impedance $Z_C = Z_W^{(\mathrm{TEM})} \cdot u^2$ can be transformed accordingly.

The geometry used is depicted in figure 5. The z axis is located in the middle of the inner conductor. Half of the cell width and accordingly outer radius are denoted $a(z)$. Considering waveguides of inherent shape, only the outer dimension is necessary, as the ratio between inner and outer dimension remains constant. For the μC^3-cell the constant ratio between outer and inner radius is $\frac{r_a}{r_i} = 2.3$ over the entire length of the cell to obtain a constant characteristic impedance of 50Ω for the TEM mode.

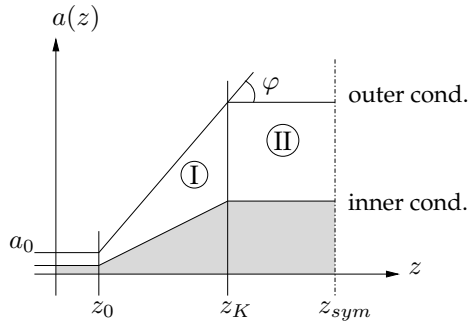

Figure 5: Geometry for resonance calculation

In region I the local outer dimension $a(z)$ is a function of z. In region II, the homogeneous middle section, a is constant. Due to symmetry the waveguide has to be described up to z_{sym} only.

The approach for $I_k^{(\mathrm{TM})}$ and $V_k^{(\mathrm{TE})}$ respectively in region I is

$$I_{k\textcircled{\scriptsize I}}^{(\mathrm{TM})} = K_1 \cdot \sqrt{a'z} \cdot J_\nu(k \cdot z) + K_2 \cdot \sqrt{a'z} \cdot J_{-\nu}(k \cdot z) \quad (6)$$

with the fractional order ν

$$\nu = \sqrt{\frac{1}{4} + \left(\frac{k_{c,norm}^{(p)}}{2a'} \right)^2} \quad (7)$$

of the Bessel function $J_\nu(k \cdot z)$ and the gradient a'

$$a' = \tan(\varphi) \quad (8)$$

of the tapered region. In region II the wave can propagate without attenuation according to

$$\begin{aligned} I_{k\textcircled{\scriptsize II}}^{(\mathrm{TM})} = {} & K_3 \cdot \cos\left(z\sqrt{k^2 - k_c^{(p)2}(z_{sym})} \right) \\ & + K_4 \cdot \sin\left(z\sqrt{k^2 - k_c^{(p)2}(z_{sym})} \right) \end{aligned} \quad (9)$$

A calculation of the four constants of integration K_1 to K_4 is possible. One constant is free of choice because the amplitude information has been lost by neglecting mode coupling. We choose $K_1 = 1$. The Bessel function with fractional order increases $J_{-\nu}(k \cdot z) \to \infty$ with negative order and small z. Because higher order modes are under cutoff for small z, $K_2 = 0$ is valid. The constants K_3 and K_4 have to adjust the transition between the tapered and the homogeneous region. Because (4) and (5) are of 2nd order at $z = z_K$ both the function and the derivative of $V^{(\mathrm{TE})}$ and $I^{(\mathrm{TM})}$ have to match. This leads to a system of equations for the remaining constants using $\overline{F_{\textcircled{\scriptsize I}}}$ and $\overline{\overline{F_{\textcircled{\scriptsize II}}}}$ according to (12) and (13).

$$\overline{F_{\textcircled{\scriptsize I}}} = \overline{\overline{F_{\textcircled{\scriptsize II}}}} \cdot \begin{pmatrix} K_3 \\ K_4 \end{pmatrix} \quad (10)$$

Solving for K_3 and K_4 results in

$$\begin{pmatrix} K_3 \\ K_4 \end{pmatrix} = \overline{\overline{F_{\textcircled{\scriptsize II}}}}^{-1} \cdot \overline{F_{\textcircled{\scriptsize I}}} \quad . \quad (11)$$

$$\overline{F_{\textcircled{I}}} = \begin{pmatrix} \sqrt{a' z_K} J_\nu(k \cdot z_K) \\ \frac{a'-2\nu a'}{2\sqrt{a' z_K}} J_\nu(k \cdot z_K) + \sqrt{a' z_K} J_{\nu-1}(k \cdot z_K) \end{pmatrix} \tag{12}$$

$$\overline{\overline{F_{\textcircled{II}}}} = \begin{pmatrix} \cos(arg) & \sin(arg) \\ -\frac{arg}{z_K}\sin(arg) & \frac{arg}{z_K}\cos(arg) \end{pmatrix} \quad \text{with} \quad arg = z_K \sqrt{k^2 - k_c^{(p)2}(z_{sym})} \tag{13}$$

$$\overline{\overline{F_{\textcircled{II}}}}^{-1} = \frac{z_K}{arg} \cdot \begin{pmatrix} \frac{arg}{z_K}\cos(arg) & -\sin(arg) \\ -\frac{arg}{z_K}\sin(arg) & \cos(arg) \end{pmatrix} \tag{14}$$

$$\begin{pmatrix} K_3 \\ K_4 \end{pmatrix} = \frac{z_K}{arg} \cdot \begin{pmatrix} \frac{arg}{z_K}\cos(arg) & -\sin(arg) \\ -\frac{arg}{z_K}\sin(arg) & \cos(arg) \end{pmatrix} \cdot \begin{pmatrix} \sqrt{a' z_K} J_\nu(k \cdot z_K) \\ \frac{a'-2\nu a'}{2\sqrt{a' z_K}} J_\nu(k \cdot z_K) + \sqrt{a' z_K} J_{\nu-1}(k \cdot z_K) \end{pmatrix} \tag{15}$$

$$I_{k\textcircled{II}}^{(\mathrm{TM})} = \sqrt{K_3^2 + K_4^2} \cdot \sin\left(z \sqrt{k^2 - k_c^{(p)2}(z_{sym})} + \arctan\left(\frac{K_3}{K_4}\right)\right) \tag{16}$$

$$\sin\left(z_{sym} \sqrt{k^2 - k_c^{(p)2}(z_{sym})} + \arctan\left(\frac{K_3}{K_4}\right)\right) = \begin{cases} 0 \\ \min/\max \end{cases} \tag{17}$$

$$z_{sym} \sqrt{k^2(f_{res}) - k_c^{(p)2}(z_{sym})} + \arctan\left(\frac{K_3(f_{res})}{K_4(f_{res})}\right) = \frac{n+1}{2} \cdot \pi \tag{18}$$

At $z = z_K$ the inverse matrix of $\overline{\overline{F_{\textcircled{II}}}}$ can be expressed by (14) which results in (15). Using the known solution for the homogeneous middle section the resonant frequency can be derived. In case of resonance the length between the two cutoff cross sections $z_c^{(p)}$ and $z_L - z_c^{(p)}$ of the waveguide is an integer multiple of half wavelength $\frac{\lambda}{2}$ which means that the symmetry of the solution in region II in (16) has to be either odd or even referring to $z = z_{sym}$. Using the resonant condition it can be concluded that the solution has to be either zero or an extremum at $z = z_{sym}$ as stated in (17).

As k, K_3 and K_4 are frequency dependent the resonant frequencies f_{res} can now be calculated with n=0,1,2,3,... using (18).

Figure 6 and 7 show the amplitude functions $I^{(\mathrm{TM})}(z)$ of TM_{01} mode for the first and second resonant frequency of TM_{01} mode in the μC^3-cell. The cell geometry is depicted with feeding section enlarging to the homogeneous middle section up to symmetry at $z = z_{sym}$. The dashed line marks the z-axis. The amplitude functions for the resonance case alternate between zero and extremum at $z = z_{sym}$ synonymous with our resonant condition. The vertical line marks the cutoff cross section showing the increasing resonant length of the cell for higher frequencies.

The resonant frequencies for the first two TM-modes can be derived using (18) in combination with the geometry of the $\mu\mathrm{C}^3$-cell [4]. They are included in table 2.

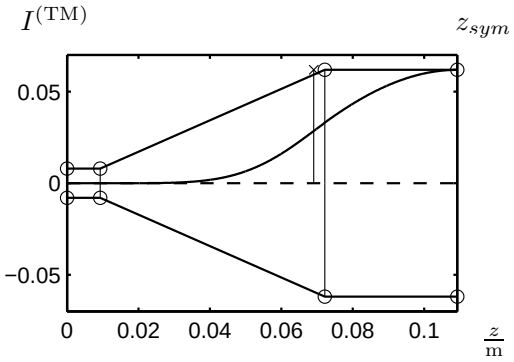

Figure 6: $I^{(\mathrm{TM})}(z)$ of TM_{01} mode for the first resonant frequency in μC^3-cell

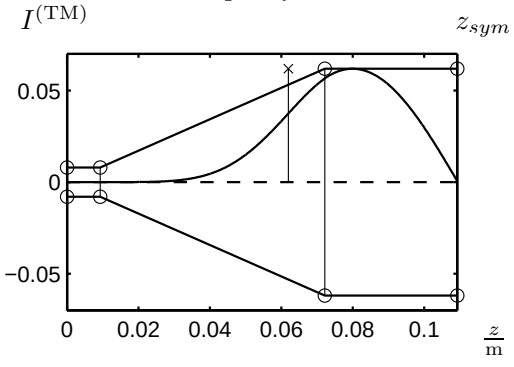

Figure 7: $I^{(\mathrm{TM})}(z)$ of TM_{01} mode for the second resonant frequency in μC^3-cell

mode	$\frac{f_{res_1}}{\mathrm{GHz}}$	$\frac{f_{res_2}}{\mathrm{GHz}}$	$\frac{f_{res_3}}{\mathrm{GHz}}$
TM_{01}	4.456	5.001	5.728
TM_{11}	4.594	5.138	5.856

Table 2: Resonant frequencies of TM_{01} and TM_{11} mode in $\mu\mathrm{C}^3$-cell up to 6 GHz, according to (18)

3 Measurements and Calculations

In order to validate the above calculations the system of generalised telegraphist's equations (1) and (2) has been calculated numerically in a frequency range $0 < f < 6$ GHz in the region $0 < z < z_L$ including TEM mode and four TM and TE modes respectively. These calculations were performed using MATLAB with the NAG toolbox. The results are depicted in Figure 8. It shows collapses of the calculated voltage coefficient $|V^{(\mathrm{TEM})}|$ of TEM mode at the output port of μC^3-cell referring to the input port at about 4.4, 5 and 5.8 GHz. This matches with the resonant frequencies in table 2. In addition measurements have been performed using a μC^3-cell. For both measurements and calculations a voltage source V is applied at the input port according to figure 4. The calculated coefficient $\frac{|V^{(\mathrm{TEM})}|}{V \cdot u/2}$ equals to S_{21} parameter. The measured S_{21} parameter of μC^3-cell is shown in figure 9. The waveguide has been modeled with FEMLAB and the RF toolbox in order to benchmark the already obtained results. S_{11} and S_{21} parameters were calculated using axial symmetry. Both are depicted in figure 10. The resonant frequencies are determined to $f_{\mathrm{TM}_{011\ldots3}} = 4.4\mathrm{GHz}, 4.9\mathrm{GHz}, 5.8\mathrm{GHz}$. Additional simulations were performed at the these frequencies using a 3D model in order to determine which mode is responsible. The results of the 3D simulation below resonance and at the very resonant frequencies are included in figure 11. The surface is coloured according to the amplitude of the longitudinal $\vec{E}$ field component. The presence of this component indicates a TM mode.

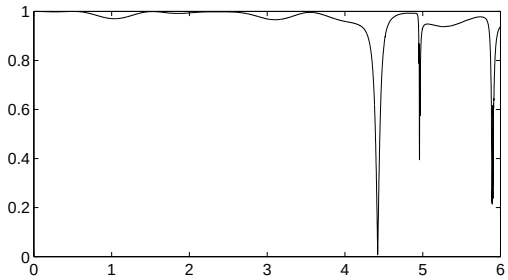

Figure 8: Simulation using generalised telegraphist's equations, MATLAB with NAG toolbox, $\frac{|V^{(\mathrm{TEM})}|}{V \cdot u/2}$, range $0 < f < 6$ GHz

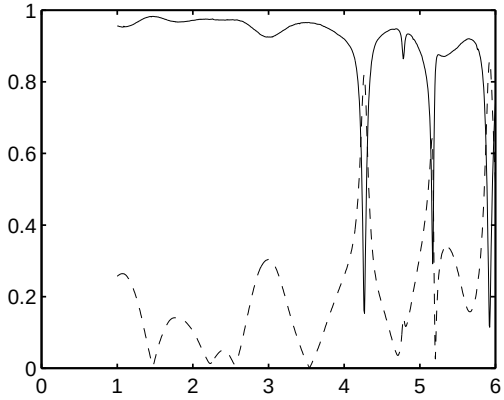

Figure 9: Measurement, S_{11}, S_{21}, range $0 < f < 6$ GHz

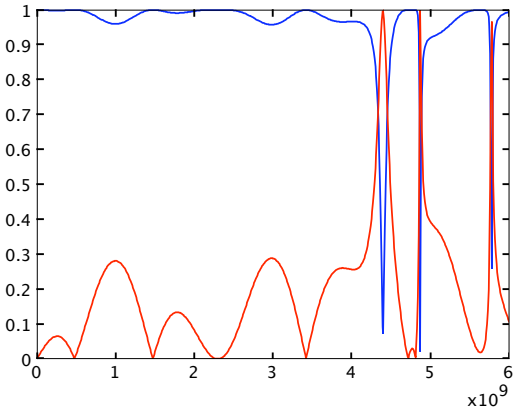

Figure 10: Simulation using FEM model, FEMLAB with RF toolbox, S_{11}, S_{21}, range $0 < f < 6$ GHz

As depicted in figures 8, 9and 10 calculated and measured resonant frequencies show close agreement.

4 Conclusion

An analytical method for the calculation of resonant frequencies of higher order modes in tapered double-port TEM waveguides has been presented. It is based on the generalised telegraphist's equations for inhomogeneous waveguides. This method allows a precise determination of the usable bandwidth for this type of TEM waveguide. Simulations can be benchmarked using this analytical method. A comparison of results obtained using two different simulation methods, 1) generalised telegraphist's equations (MATLAB with NAG toolbox) and 2) FEM model (FEMLAB with RF toolbox) show close agreement.

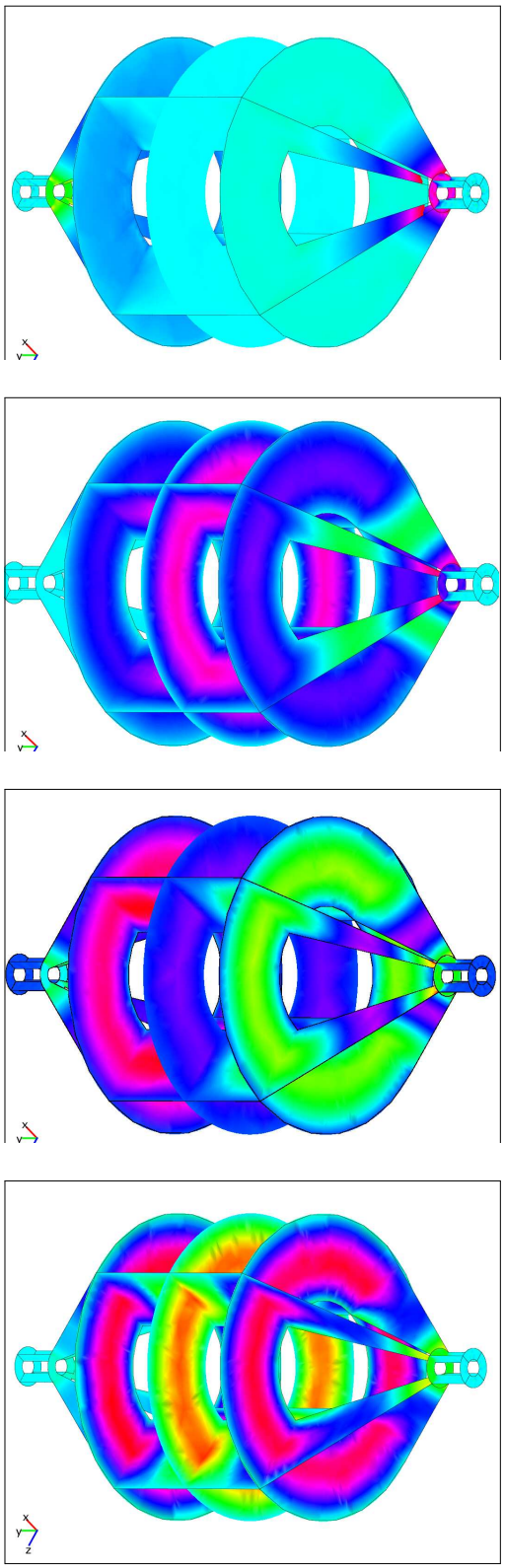

Figure 11: Longitudinal component of the electric field, top to bottom: $f = 1$ GHz, $f_{\mathrm{TM}_{011}} = 4.4$ GHz, $f_{\mathrm{TM}_{012}} = 4.9$ GHz, $f_{\mathrm{TM}_{013}} = 5.8$ GHz

References

[1] M.L. Crawford, *Generation of standard EM fields using TEM transmission cells* IEEE Trans. on EMC, Vol. EMC-16, 1974, pp. 189-195.

[2] J. Glimm, K. Münter, R. Pape, Th. Schrader, M. Spitzer, *The New National Standard of EM Field Strength; Realization and Dissemination*, Proceedings 12th International Zurich Symposium and Technical Exhibition on EMC, Zurich, Switzerland, 18-20 February, 1997, pp. 611-613.

[3] C. Groh, J.P. Kärst, M. Koch, H. Garbe, *TEM Waveguides for EMC Measurements* IEEE Trans. on EMC, Vol. EMC-41, No. 4, November 1999, pp. 440-445.

[4] J.P. Kärst, C. Groh, H. Garbe, *Calculable Field Generation using TEM Cells Applied to the Calibration of a Novel E Field Probe* IEEE Trans. on EMC, Vol. EMC-44, No. 1, February 2002, pp. 59-71.

[5] Ch. Groh, *TEM-Zellen zur Kalibration von elektromagnetischen Feldsensoren* , Ph.D. Thesis, University of Hanover, Fortschritt-Bericht Reihe 21 Nr. 327, Düsseldorf, VDI Verlag 2002

[6] J.P. Kärst, *Qualifikation beladener TEM-Wellenleiter* , Ph.D. Thesis, University of Hanover, Fortschritt-Bericht Reihe 21 Nr. 329, Düsseldorf, VDI Verlag 2002

[7] S.A. Schelkunoff, *Conversion of Maxwell's Equations into Generalized Telegraphist's Equations*, Bell. Sys. Tech. Jour. 34, 1955, pp. 532-579.

[8] G. Reiter, *Generalized Telegraphist's Equation for Waveguides of Varying Cross-Section*, Proc. of the IEE Vol 106 B Supplement 13, 1959, pp. 54-61.

[9] F. Sporleder, H.G. Unger, *Waveguide Tapers Transitions and Couplers*, IEE Wave Series 6, London, New York, 1979.

[10] N. Marcuwitz, *Waveguide Handbook*, Peter Peregrinus Ltd, IEE Electromagnetic Wave Series 21, 1986 Edition